ACS SyntheticBiology

pubs.acs.org/synthbio

Research Article

Design of Four Small-Molecule-Inducible Systems in the Yeast Chromosome, Applied to Optimize Terpene Biosynthesis

Jong Hyun Park, Marcelo C. Bassalo, Geng-Min Lin, Ye Chen, Hamid Doosthosseini, Joep Schmitz, Johannes A. Roubos, and Christopher A. Voigt*

Cite This: *ACS Synth. Biol.* 2023, 12, 1119–1132

Read Online

ACCESS | Metrics & More | Article Recommendations | Supporting Information

ABSTRACT: The optimization of cellular functions often requires the balancing of gene expression, but the physical construction and screening of alternative designs are costly and time-consuming. Here, we construct a strain of *Saccharomyces cerevisiae* that contains a "sensor array" containing bacterial regulators that respond to four small-molecule inducers (vanillic acid, xylose, aTc, IPTG). Four promoters can be independently controlled with low background and a 40- to 5000-fold dynamic range. These systems can be used to study the impact of changing the level and timing of gene expression without requiring the construction of multiple strains. We apply this approach to the optimization of a four-gene heterologous pathway to the terpene linalool, which is a flavor and precursor to energetic materials. Using this approach, we identify bottlenecks in the metabolic pathway. This work can aid the rapid automated strain development of yeasts for the bio-manufacturing of diverse products, including chemicals, materials, fuels, and food ingredients.

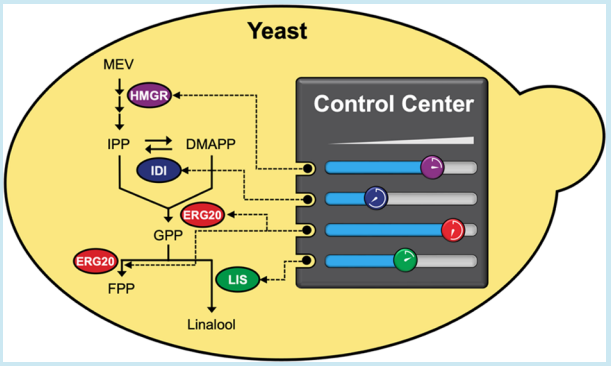

KEYWORDS: *synthetic biology, systems biology, Escherichia coli Marionette, design-build-test-learn (DBTL) cycle, fungi, genetic circuit, high energy aircraft missile fuel*

INTRODUCTION

Saccharomyces cerevisiae is commonly used for bio-manufacturing high-value products by introducing pathways from plants, animals, other fungi, and bacteria.[1−9] These pathways have gotten large that involve dozens of genes, that must be carefully tuned to enhance metabolic flux, deliver electrons, and avoid the accumulation of toxic intermediates.[5,10−15] Regulatory circuits can dynamically coordinate their production to when they are needed or avoid toxic intermediates or byproduct accumulation.[16−18] There are now large libraries of *S. cerevisiae* genetic parts available to control expression, including promoters, untranslated regions (UTRs), and terminators.[14,19−27] These parts can be used to optimize a multigene system by creating a library where genes are placed under the control of parts of different strengths to "sweep" through expression space.[19,28−32] The search space is large and highly dimensional, so approaches based on design of experiments (DOE), machine learning (ML), or metabolic modeling have been applied to accelerate the search.[33−40] However, the creation of large libraries of DNA constructs is expensive and slow and is much lower throughput than the capabilities of automated screening and characterization platforms.[29,39,41−44]

Inducible systems based on small-molecule sensors can tune gene expression over orders of magnitude. Many sensors have been built for yeast and other organisms by introducing a heterologous DNA-binding regulatory protein and then placing the operator in a scaffold of a constitutive promoter.[1,23,24,45−55] Sensors are more stable and reliable when they are carried in the genome, as opposed to plasmids.[54] The response function of the sensor captures how the activity of the output promoter changes with the addition of the small-molecule input. Sensors have been developed for *S. cerevisiae* that respond to anhydrotetracycline (aTc), xylose (Xyl), isopropyl-*β*-D-thiogalactoside (IPTG), vanillic acid (Van), 2-4-diacetylphloroglucinol (DAPG), salicylate, adipic acid, naringenin (Nar), cumate (CumA), 3-oxo-hexanoyl homoserine lactone (OC6), camphor, progesterone, estradiol, aldosterone, testosterone, 1,2-bis(4-hydroxyphenyl)ethane-1,2-dione (DHB), and dexamethasone.[52,53,56−65] However, to work together in a single cell, the sensors must be orthogonal; in other words, the small molecules cannot bind to off-target regulators and the regulators must bind to unique DNA sequences.[56,66−69] Several groups have combined three sensors in a single

Received: November 10, 2022
Published: March 21, 2023

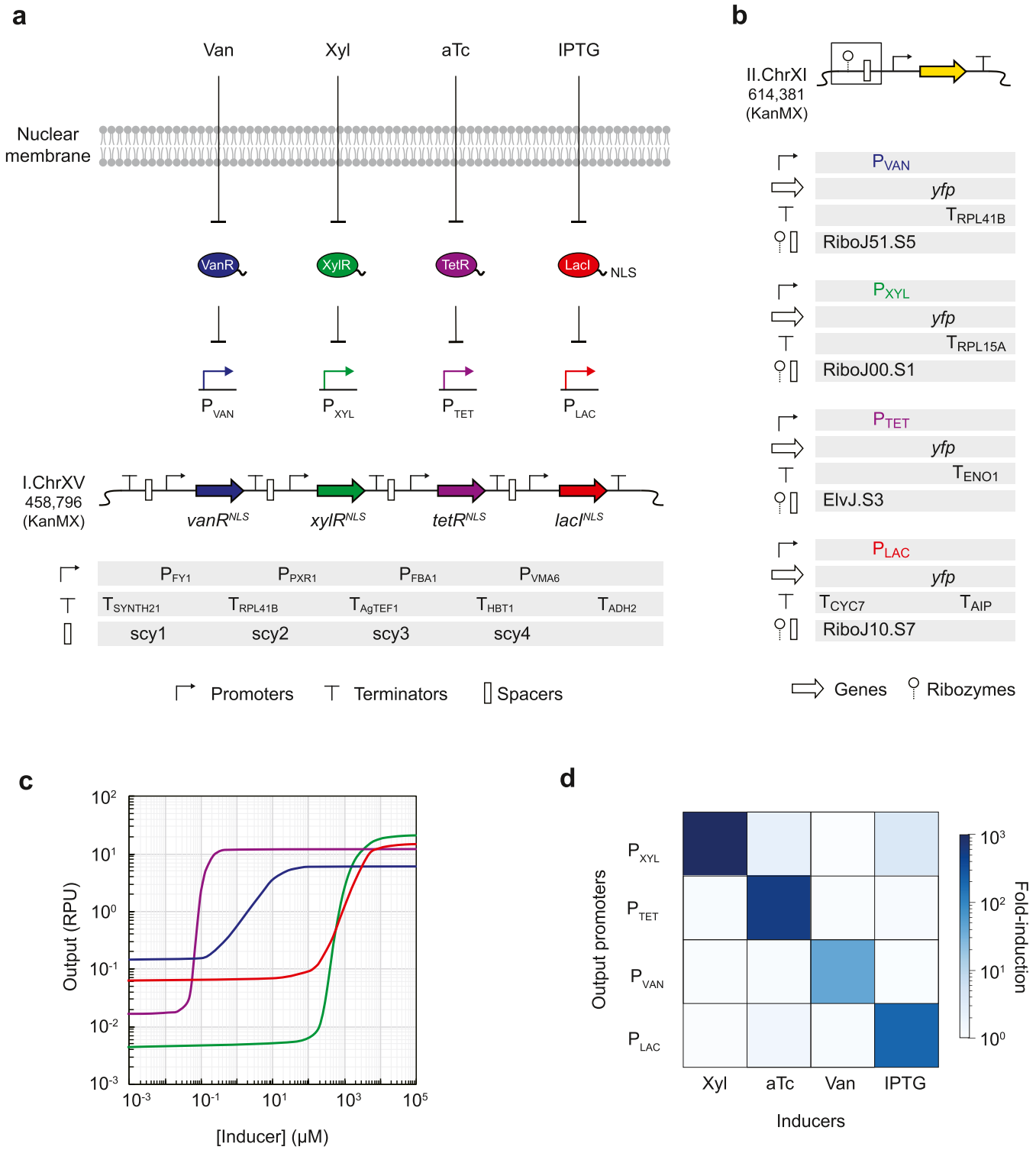

Figure 1. Four inducible systems in the *S. cerevisiae* genome. (a) Schematic of the sensor array and corresponding parts (sequences provided in Tables S5–S8). The sensor array was integrated in Chromosome XV between 458 198 and 459 658 (INT1) in *S. cerevisiae* BY4741 to make *S. cerevisiae* MBY07. Full strain genotypes are provided in Table S8. (b) Constructs to measure sensor outputs. The four output promoters were fused to *yfp* and used to make strains *S. cerevisiae* MBY58, MBY59, MBY60, and MBY61. (c) Response functions for each inducible system. The response functions were obtained by fitting the data to eq 1, the parameters for which are shown in Table 1. Three replicates were performed on different days (Note S1). (d) Orthogonality of the inducible systems. The strains containing the sensor array and each of the four output promoters were induced with 20 mM Xyl, 200 ng/mL aTc, 50 μM Van, or 20 mM IPTG (Methods). The fold-induction was calculated by dividing the geometric mean fluorescence in the presence of inducer by that of cells grown in its absence. The means of three replicates performed on different days are shown here, and all of the data are provided in Figure S2.

strain.[56,61,63,70] Khalil and co-workers demonstrated that four hormone sensors could be incorporated into the yeast chromosome and applied to optimize a biosynthetic pathway to produce violicin.[65]

https://doi.org/10.1021/acssynbio.2c00607
ACS Synth. Biol. 2023, 12, 1119−1132

Normalizing the promoter activity by a reference promoter of known strength allows it to be reported in relative promoter units (RPU).[56,71−73] Previously, we defined PFY1 as the yeast reference promoter for the calculation of RPU.[56] When a sensor's output is provided in RPU, it is possible to calculate how it can be connected to a downstream genetic circuit. It also aids computational search algorithms designed to sweep efficiently through expression space. Additionally, promoters can be swapped of the same strength, for example, exchanging an inducible promoter (at a defined inducer concentration) for a constitutive promoter of the same strength. This procedure can be performed after optimization to create a strain for biomanufacturing that does not require the addition of inducers.[74]

In addition, the timing of gene expression can be important for optimizing product titer.[18,75−77] For example, there is a need to balance between the needs of biomass accumulation and product formation.[78] To address this, sensors have been developed in *Escherichia coli* to turn on at late stages of growth.[18,79,80] "Just-in-time" expression is a theory that enzymes that act early in a pathway should be expressed before those that act later.[81] This ordering is beneficial when there is the potential for futile cycles of enzyme expression and degradation.[81−83]

To demonstrate optimization, we selected a linalool biosynthetic pathway developed for *S. cerevisae*.[84−86] Linalool is a monoterpene alcohol with a floral aroma that is an ingredient in foods, cosmetics, and pharmaceuticals. Linalool can also be catalytically converted to high energy fuels (RJ-4, used in Tomahawk cruise missiles).[87−90] To produce linalool, the metabolite mevalonate (MEV) is converted to mevalonate-5-phosphate (MEV-5P) by HMG-CoA Reductase (tHMGR), which has been observed to be a bottleneck and whose overexpression is a common optimization strategy.[84−86,91,92] In the native MEV pathway of *S. cerevisiae*, MEV-5P is converted to isopentenyl phosphate (IPP) and dimethylallyl pyrophosphate (DMAPP), whose distribution is controlled by isopentenyl diphosphate isomerase (IDI).[93] IPP and DMAPP are converted to geranyl pyrophosphate (GPP) by farnesyl pyrophosphate synthase (ERG20). GPP is converted to linalool by linalool synthase (LIS). LIS from *Mentha citrata* has been used for recombinant expression with an N-terminal truncation (t67-McLIS) to prevent plastid targeting.[94,95] ERG20 competes with this product by converting GPP to farnesyl pyrophosphate (FPP). Therefore, reducing ERG20 expression or mutating it to reduce FPP production (ERG20*, where * indicates F96W/N127W) increases linalool titers.[84,92,96,97] When enzymes are mis-expressed, toxic intermediates can accumulate, leading to slower growth and lower titer.[88,92] Linalool production has also been optimized by overexpressing the MEV pathway and reducing the expression of native enzymes at the entry of metabolic branch points.[86,92]

In this manuscript, we describe the combination of four small-molecule sensors (aTc, IPTG, Van, and Xyl) into a single "sensor array" that is inserted into the chromosome of *S. cerevisiae*. The four sensors are shown to produce large dynamic ranges, low background, minimally impact growth rate, and are orthogonal. The four sensors are used to drive the expression of different enzymes in the linalool pathway (tHMGR, IDI, ERG20*, t67-McLIS). This strain was used to evaluate combinations of inducers to optimize the linalool titer. Further, each gene was induced at a different time to determine the impact of expression dynamics. This approach demonstrates the rapid optimization of the levels and timing of gene expression using an array of inducible systems.

RESULTS

S. cerevisiae with a Four Genome-Encoded Inducible System. The design of the strain containing the sensor array is shown in Figure 1a. Each sensor consists of a repressor protein and an output promoter. The repressor genes are encoded together in the INT1 locus of chromosome XV in *S. cerevisiae* BY4741 (Figure S1). The repressors are codon-optimized for yeast expression and are fused to a C-terminal nuclear localization signal (NLS). The genes are expressed from strong constitutive promoters. Strong terminators block transcriptional read-through between the genes.[56] Different genetic parts were selected for each cistron to avoid regions of sequence identity that can lead to homologous recombination and genomic instability. The array was assembled using a hierarchical cloning strategy followed by a CRISPR/Cas9-assisted genome integration (Methods) (Table S1).[98,99]

The output promoters of the sensors are P_{XYL}, P_{TET}, P_{VAN}, and P_{LAC}. Four reporter strains were constructed to measure their response (Note S1 and Table S2). Each contains an output promoter fused to the yellow fluorescent protein gene (*yfp*) (Figure 1b). The constructs were integrated into the INT2 locus on Chromosome XI (Figure S1). The cells were grown with their inducer for 24 h in SD medium and fluorescence was quantified using flow cytometry (Methods). The arbitrary units of fluorescence obtained by cytometry were normalized by the fluorescence from the PFY1 reference promoter to report the data in relative promoter units (RPU) (Methods). The induction data were fit to the response function

$$y = y_{min} + (y_{max} - y_{min})\frac{x^n}{K^n + x^n} \quad (1)$$

where x is the inducer concentration, n is the cooperativity, K is the threshold, y is output promoter activity (in RPU), and y_{min}/y_{max} are the minimum/maximum promoter activities (Table 1). The fold-inductions obtained from the Van, Xyl, aTc, and IPTG sensors were 40-, 5000-, 1000-, and 240-fold, respectively (Figure 1c and Table 1). The orthogonalities of the four sensors were tested and almost no off-target activities were observed (Figure 1d). These data indicate that the inducible systems can be used to independently control the expression of different genes over a wide dynamic range. We measured the impact on growth rate in the presence and absence of inducers compared to the wild-type strain (Note S1). The strains with and without the sensors grow similarly and were not impacted by the addition of the inducers.

Table 1. Inducible System Parameters

sensor	y_{min} (RPU)[a]	y_{max} (RPU)	K (μM)	n
IPTG	0.06	15	4.5	1.6
Xyl	0.004	22	3.4	1.6
aTc	0.01	12	51	4.9
Van	0.15	6	8.6	1.3

[a]The parameters were obtained from fits to eq 1.

Linalool Optimization through Inducible Enzyme Control. Four enzymes in the linalool biosynthetic pathway were placed under the control of different inducible systems (Figure 2a) and a strain was constructed that places these

https://doi.org/10.1021/acssynbio.2c00607
ACS Synth. Biol. 2023, 12, 1119−1132

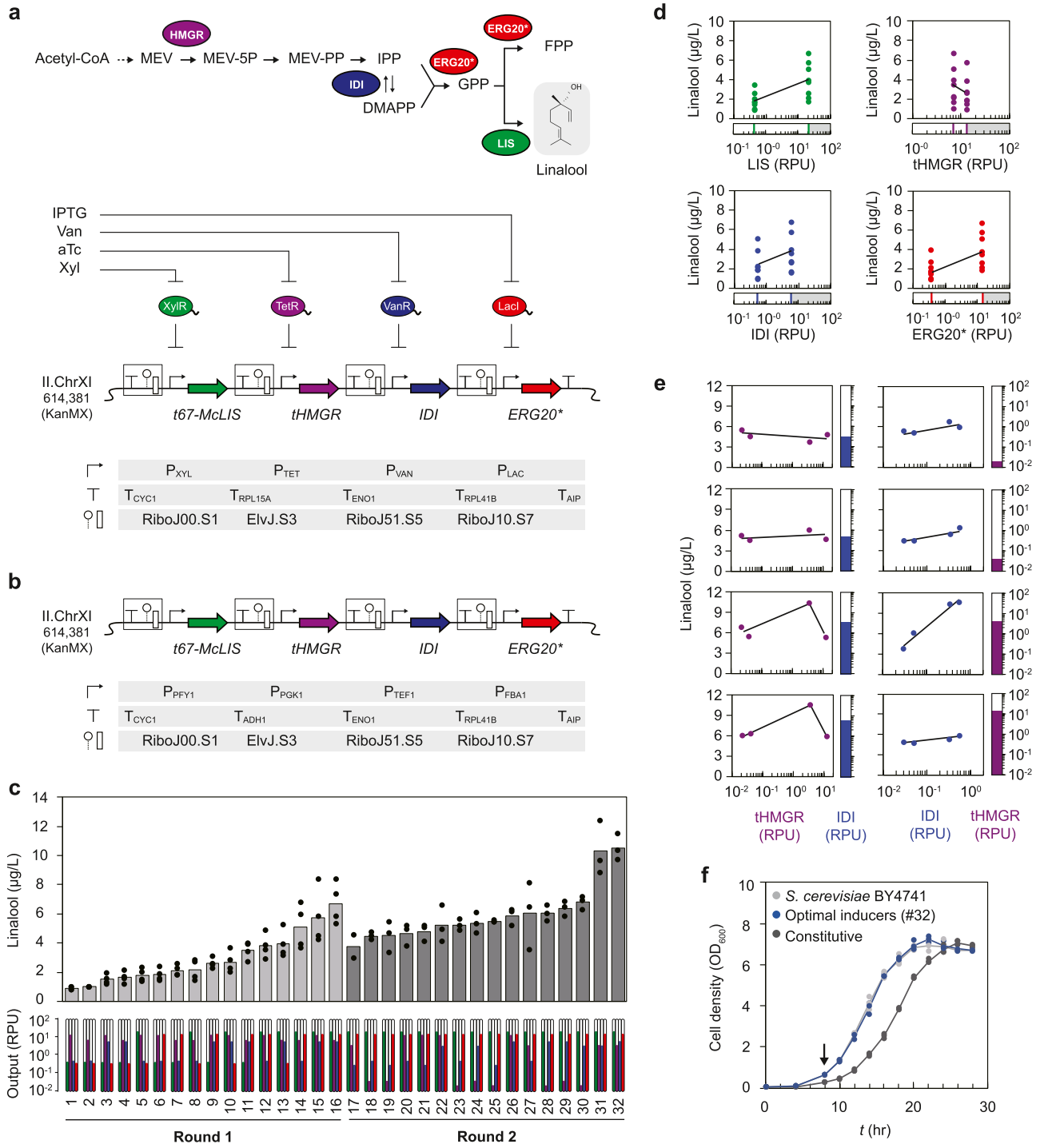

Figure 2. Optimization of linalool titers by changing expression levels. (a) The metabolic pathway for linalool biosynthesis is shown, highlighting the enzymes placed under inducible control (colored by the inducible system used). The genetic system to control the targeted genes with individual sensor promoters is shown (part sequences provided in Table S8). The parts labeled xx.S# are insulators designed with ribozyme/spacer combinations to block errant upstream transcription.[56] (b) "Constitutive" strain (*S. cerevisiae* MBY62) has the enzyme genes under the control of constitutive promoters. (c) Effects of different combinations of inducers on linalool production. The bottom scale represents the expression levels of each gene, based on the activity of the inducible promoter in RPU. Four replicates were performed on different days (dots), and the bars show the means of these values. Inducer concentrations are provided in the main text, and values are provided in Table S3. (d) Regression analysis of linalool production versus the expression of each individual gene in Round 1. Each marker represents one sample with different inducer combinations of inducers. The enzymes are shown with the expression levels from their corresponding inducible promoters. (e) Effect of increasing tHMGR (left) and IDI (right) expression on linalool titers, with the other enzyme expression held constant (shown as a bar and increasing from top to bottom). (f) Growth comparison between the wild type (*S. cerevisiae* BY4741), the addition of optimal inducer concentrations (#32) at time = 8 h (arrow) (*S. cerevisiae* MBY63), and when the enzymes are under constitutive control (*S. cerevisiae* MBY62). Three replicates are shown, and the curves pass through the means of these points.

https://doi.org/10.1021/acssynbio.2c00607
ACS Synth. Biol. 2023, 12, 1119−1132

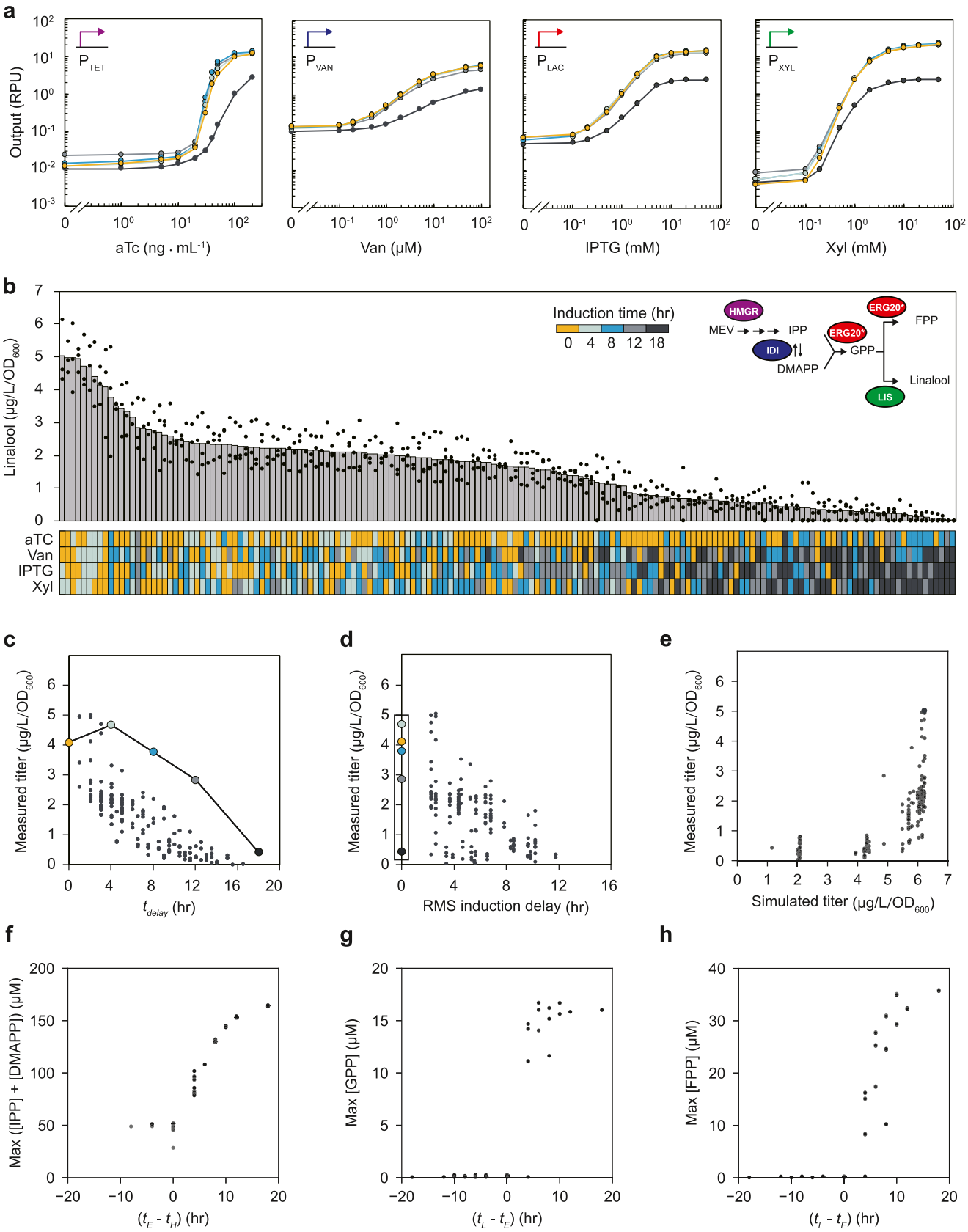

Figure 3. Impact of controlling the timing of expression. (a) Response of each sensor induced at different times (0, 8, 12, or 18 h) (*S. cerevisiae* MBY58, MBY59, MBY60, and MBY61). The means of three replicates, performed on different days, are shown with the raw data provided in Figure S5. Each induction time is represented by different colors as shown in the inset of (b). (b) Normalized linalool titers for the combinations of induction times. The concentrations of inducers were 20 mM Xylose, 100 ng/mL aTc, 50 μM vanillic acid, and 20 mM IPTG. A minimum of three experiments were performed on different days (dots), and the bars are the means of these measurements. Detailed conditions of each experiment are summarized in Table S4. (c) Effect of delayed expression for each enzyme. The average of the induction times for the enzymes $t_{delay} = \langle t_H + t_I +$

https://doi.org/10.1021/acssynbio.2c00607
ACS Synth. Biol. 2023, 12, 1119−1132

Figure 3. continued

$t_E + t_L$⟩. Colored dots indicate when all inducers were added at the same time (e.g., $t_H = t_I = t_E = t_L = 4$ h) following the color code of the inset of (b). (d) Impact of asynchronous expression. The root-mean-square variation was calculated as: RMS = $(1/6)\sqrt{[(t_H - t_I)^2 + (t_H - t_E)^2 + (t_H - t_L)^2 + (t_I - t_E)^2 + (t_I - t_L)^2 + (t_E - t_L)^2]}$. Colored and boxed dots indicate when all inducers were added at the same time following the color code of the inset of (b). (e) Simulated linalool titers compared with the experimentally measured titers. (f) Maximum level of the sum of the intermediates IPP and DMAPP over the course of each simulation varying the induction times. The data are plotted versus the difference of the induction times of ERG20* and tHMGR ($t_E - t_H$). (g) Maximum concentration of GPP for each simulation varying the induction times as a function of the difference in LIS and ERG20* induction times ($t_L - t_E$). (h) Maximum concentration of FPP for each simulation varying the induction times as a function of the difference in LIS and ERG20* induction times ($t_L - t_E$).

enzymes under the control of strong constitutive promoters (Figure 2b). Strong terminators and ribozyme-based insulators were placed between the genes to avoid read-through or nucleosome effects, where the induction of one system would impact neighboring genes.[66,100,101] The pathway was integrated into the INT2 genomic locus to create *S. cerevisiae* MBY63 (Figure S1). Linalool production was measured by growing the strains for 48 h in SD medium under inducing conditions (Methods). Linalool production was measured through solid-phase microextraction followed by gas chromatography-mass spectrometry (SPME-GC/MS) and the titer quantified by dividing the linalool peak area by the internal standard (IS, Caryophyllene) peak area (Methods). This internal standard has been previously demonstrated to improve the measurement reproducibility between replicates by controlling for errors during sample preparation.[102,103] Upon maximum induction by all of the inducers, linalool begins to accumulate after 12 h and plateaus at 36 h (Figure S3).

We varied the expression levels of the four enzymes using a two-level factorial design. This technique and similar optimization algorithms have been applied to the optimization of metabolic pathways, but where the variants are constructed using DNA synthesis and assembly leading to libraries as large as 2 MB.[33,34,36,38] Two levels of expression were selected for each enzyme (low/high): 0.5/20 mM Xyl, 60/200 ng/mL aTc, 1/50 μM Van, and 0.5/20 mM IPTG. This corresponds to the following promoter activities: 0.4/21.0, 7.0/13.1, 0.5/5.7, 0.4/14.3 RPU. Cultures were grown in SD medium for 48 h, with inducers added after 8 h (Methods). We sampled this combinatorial set of expression levels ($2^4 = 16$ combinations) and identified combinations that led to the highest linalool production levels ("Round 1," Figure 2c).

A linear regression analysis was performed to extract the contribution of each gene on the linalool titer (Figure 2d). Higher expression levels of LIS and ERG20* correlated with high linalool titers. In contrast, higher expression of tHMGR had a detrimental effect on linalool production. Considering the role of tHMGR in increasing flux in the MEV pathway,[104−106] this result could indicate an imbalance between upstream flux and downstream precursor consumption.

Then, we performed a second round of optimization. We set the expression levels of LIS and ERG20* to the high level and fine-tuned the expression of IDI and tHMGR ("Round 2," Figure 2c and Table S3). This led to an increase in the titer by identifying the optimal intermediate levels of both enzymes. Further, this revealed an interdependency between the optimal tHMGR and IDI expression levels. Increasing the expression of tHMGR increased the linalool titer only after IDI passed a threshold (Figure 2e). Below this threshold, the titer is independent of tHMGR expression and above it, an intermediate IDI level was optimal, and this remained the same even when tHMGR was increased further. Interestingly, the titer was independent of IDI at both low and high levels of tHMGR expression. Only at an intermediate expression level, did increases in IDI lead to increased titer. This indicates that both tHMGR and IDI need to have their expression levels balanced to improve linalool production. Only when there was sufficient flux into the mevalonate pathway, IDI contributed with increased IPP and DMAPP supply.

The optimal linalool production was obtained from the following inducer concentrations: 20 mM Xyl, 100 ng/mL aTc, 50 μM Van, and 20 mM IPTG (#32 in Figure 2c). We also compared the linalool titer between when the enzymes were under inducible control, with optimal levels of inducers (#32) (9.9 ± 0.3 μg/L), to when they were constitutively expressed (6.0 ± 0.8 μg/L). One reason for this difference is that the constitutive expression of the enzymes decreased the growth rate, even though they were expressed from promoters that are slightly weaker than the inducible promoters at the tested levels. The inducible system allows expression to be delayed so that cell growth can be seeded, thus allowing a higher titer to be achieved (Figure 2f).

Optimization of Enzyme Expression Timing. Because the delay in enzyme expression improved growth, we decided to explore the effects of changing the order and timing. These experiments can be performed easily by changing when inducer is added to the culture. First, we characterized the dynamics of the four inducible systems. We added inducers at 0, 4, 8, 12, or 18 h after cells were inoculated into fresh SD medium (Methods). The response functions were measured after the cells were induced for different lengths of time (Figure 3a). There was a large difference when the induction was delayed to 18 h, after cells have entered stationary phase.

We then tested different induction times to optimize the linalool titer. Experiments were performed where each inducer was added at different times, resulting in 166 combinations (Figure 3b). The highest titer was obtained when there was a 4 h delay in the last two steps of the pathway (ERG20* and LIS). We also observe that higher titers were obtained when all inducers were added simultaneously. Figure 3c shows the total delay t_{delay} as the sum of the delays for each enzyme. The line shows the titer obtained when all four enzymes were expressed at times 0, 4, 8, 12, and 18 h. The simultaneous expression of the enzymes was consistently beneficial. This effect was also observed with the root mean square (RMS) of the delays, where more variable induction timing tended to produce lower titers (Figure 3d). It was known that the accumulation of intermediates in the MEV pathway can have a toxic effect on the host strain.[107−110] Specifically, HMG-CoA accumulation negatively impacts fatty acid biosynthesis[107,108] and high IPP inhibits growth and reduces glucose uptake.[109,110] It may be that it is important to induce all enzymes simultaneously to avoid the accumulation of these intermediates.

https://doi.org/10.1021/acssynbio.2c00607
ACS Synth. Biol. 2023, 12, 1119−1132

Simulations were performed to explore the relationship between induction times, linalool titer, and the accumulation of pathway intermediates. The expression of each enzyme was solved analytically. For example, considering tHMGR expressed at time t_H

$$\frac{d[tHMGR]}{dt} = \begin{cases} \alpha y_{min}^{TET} - \gamma[tHMGR] & t < t_H \\ \alpha y^{TET} - \gamma[tHMGR] & t \geq t_H \end{cases} \quad (2)$$

where y^i is the output promoter activity of inducible promoter P_i at the inducer concentration used and min refers to the uninduced activity (in RPU) (eq 1). The dilution rate γ = 0.00577 min^{-1} was assumed to be dominated by cell division, and the conversion factor α = 0.0028 μM/min-RPU was estimated from values obtained from the literature.[56,111,112] Analytical solutions to eq 2 are

$$[tHMGR] = \frac{\alpha y_{min}^{TET}}{\gamma}, \quad t < t_H \quad (3)$$

and

$$[tHMGR] = \frac{\alpha y^{TET}}{\gamma} + C_1 e^{-\gamma t}, \quad t \geq t_H \quad (4)$$

where C_1 is the integration constant obtained by implementing the initial condition

$$[tHMGR] = \frac{\alpha y_{min}^{TET}}{\gamma} \text{ at } t = t_H \quad (5)$$

yielding

$$C_1 = \frac{\alpha(y_{min}^{TET} - y^{TET})}{\gamma} e^{\gamma t_H} \quad (6)$$

and finally

$$[tHMGR] = \frac{\alpha}{\gamma}[y^{TET} + (y_{min}^{TET} - y^{TET})e^{-\gamma(t-t_H)}], \quad t \geq t_H \quad (7)$$

Similar equations were derived for [IDI], [ERG20], and [LIS], which were induced at times t_I, t_E, and t_L at promoter strengths y^{VAN}, y^{LAC}, and y^{XYL}, respectively. The parameters α and γ were assumed to be the same for the inductions of all enzymes.

Ordinary differential equations were then used to simulate the change in concentrations of the linalool pathway intermediates. The enzymes were assumed to follow Michaelis–Menten kinetics, described with a k_{cat} (k_i^f and k_i^r for forward and reverse, where i is the first letter of the enzyme) and K_M ($K_{i,j}$ where i is the enzyme and j the metabolite). tHMGR was assumed to operate with an excess of substrate (HMG-CoA)[113] and to be the rate-limiting step in IPP production.[114−116] The production and use of IPP can thus be written as

$$\frac{d[IPP]}{dt} = k_H^f[tHMGR] + \frac{k_I^r[IDI][DMAPP]/K_{I,D} - k_I^f[IDI][IPP]/K_{I,I}}{1 + [DMAPP]/K_{I,D} + [IPP]/K_{I,I}} - \frac{k_{E,1}^f[ERG20^*][DMAPP][IPP]}{(K_{E,D} + [DMAPP])(K_{E,I} + [IPP])} - \frac{k_{E,2}^f[ERG20^*][GPP][IPP]}{(K_{E,G} + [GPP])(K_{E,I} + [IPP])} - \gamma[IPP] \quad (8)$$

Each subunit of ERG20*, which homodimerizes, contains an active site.[117,118] Thus, rate equations for a bi-reactant mechanism[119] with independent reactant affinity[120] were used, where subscripts of $k_{E,1}$ and $k_{E,2}$ refer to the production of GPP (1) or FPP (2) and the subscripts of $K_{E,D}$, $K_{E,I}$, and $K_{E,G}$ capture the different substrates dissociating from this enzyme.[115,118] Similarly, the following equations describe the dynamics of the remaining pathway metabolites

$$\frac{d[DMAPP]}{dt} = \frac{-k_I^r[IDI][DMAPP]/K_{I,D} + k_I^f[IDI][IPP]/K_{I,I}}{1 + [DMAPP]/K_{I,D} + [IPP]/K_{I,I}} - \frac{k_{E,1}^f[ERG20^*][DMAPP][IPP]}{(K_{E,D} + [DMAPP])(K_{E,I} + [IPP])} - \gamma[DMAPP] \quad (9)$$

$$\frac{d[GPP]}{dt} = \frac{k_{E,1}^f[ERG20^*][DMAPP][IPP]}{(K_{E,D} + [DMAPP])(K_{E,I} + [IPP])} - \frac{k_L[LIS][GPP]}{K_L + [GPP]} - \frac{k_{E,2}^f[ERG20^*][GPP][IPP]}{(K_{E,G} + [GPP])(K_{E,I} + [IPP])} - \gamma[GPP] \quad (10)$$

$$\frac{d[FPP]}{dt} = \frac{k_{E,2}^f[ERG20^*][GPP][IPP]}{(K_{E,G} + [GPP])(K_{E,I} + [IPP])} - \gamma[FPP] \quad (11)$$

$$\frac{d[Linalool]}{dt} = \frac{k_L[LIS][GPP]}{K_L + [GPP]} - \gamma[Linalool] \quad (12)$$

which assume that the production of linalool only occurs in the forward direction and additional sources and sinks of these compounds in the greater metabolic network are negligible. Most of the kinetic rate constants (k_H^f = 0.186, k_I^f = 456.8, k_I^r = 667, $k_{E,1}$ = 0.072, $k_{E,2}$ = 0.126, k_L = 14.4 min^{-1}) and Michaelis constants ($K_{I,I}$ = 43, $K_{I,D}$ = 43, $K_{E,I}$ = 4.7, $K_{E,D}$ = 0.049, $K_{E,G}$ = 27.6, K_L = 25 μM) were obtained from the literature.[114−116,118,121,122] The simulated linalool concentration (in μM) was converted to a titer (in μg/L) using the following equation: titer = $V N M_l c \times 10^{-12}$, where V is the cell volume (42 μm^3), N = 1.5 × 10^7 cells/mL, and the linalool molecular weight M_l = 154.25 g/mol. The simulations correlated well with the experimental data (Figure 3e). Some combinations of inducer timings were predicted to lead to a higher titer than we observe experimentally (bottom right of Figure 3e), likely

https://doi.org/10.1021/acssynbio.2c00607
ACS Synth. Biol. 2023, 12, 1119−1132

because we are not including the impact of the accumulation of pathway intermediates on growth or regulatory feedback.

From the simulations, we inferred the concentrations of the intermediates to develop a better understanding of how the enzyme expression timing impacts linalool titer. Specifically, we explored the role of synchronous induction in leading to a higher titer. This result was grossly replicated by the simulations, and we could use these data to determine the role of enzyme expression order on the accumulation of intermediates. Of all of the possible combinations of timing orders, we found two that led to the accumulation of intermediates (Figure 3f−h). Delaying induction of ERG20* so that it occurs after tHMGR increases the intracellular concentrations of IPP and DMAPP (Figure 3f). These intermediates are known to be toxic when they overaccumulate in the cell.[109,110] Similarly, delaying the expression of LIS to occur after ERG20* leads to the accumulation of the intermediate GPP and the diversion of the flux to the unwanted alternative product FPP (Figure 3g,h). Therefore, the model predicts that it is detrimental to delay the expression for enzymes that occur later in the pathway, but there is no problem with expressing them too early with respect to the long delay times. The only detrimental effect to expressing later enzymes too early would be to create a "futile cycle" where they are degraded before they can perform their function. This effect was not accounted for in our model and we do not observe this impact experimentally. The simulations support the conclusion that the enzyme expression should be delayed to obtain higher growth and all enzymes be expressed simultaneously to avoid the production of intermediates.

DISCUSSION

Sensors that respond to small molecules offer the ability to sweep through expression levels to evaluate the impact on a cellular system. They have been central to advances in understanding natural processes in the cell as well as building and optimizing synthetic systems. Many of the early advances in synthetic biology came due to the plasmid system of Lutz and Bujard that allowed for the easy simultaneous use of three inducible (IPTG, aTc, and Ara) systems in *E. coli*.[123] Their modular structure facilitated the design of early genetic circuits and were applied more broadly to understanding the impact of expression on metabolic pathways and molecular machines.[124,125] To have similar impact, a system should be easy-to-use and characterized in units that are interpretable by other labs. Here, we have developed a system of four inducible systems for yeast, encoded in the genome, optimized to sweep through large dynamic ranges, and characterized in RPU.

It is important that the inducible systems do not interfere with each other, otherwise the impact on the system would be hard to deconvolute. In part, this property has been achieved using regulators that do not bind to each other's molecules or DNA sequences.[56,126] In yeast, there is the additional problem where it is difficult to block the transcription that occurs between neighboring cistrons. We overcome this problem by placing insulators between the genes so that each inducible system only impacts the expression of its assigned enzyme without having to spatially separate the loci across the genome.

Previously, we developed a strain of *E. coli* that contains 12 inducible systems encoded in its genome, which we refer to as the "Marionette" strains because so many genes can be simultaneously controlled. Additional inducible systems were not added, in part, because we began to observe a growth burden that would affect its use to optimize systems. In yeast, there are additional regulatory proteins that are orthogonal to the four that we selected, but we began to observe a growth defect with larger numbers of inducible systems. In theory, it should be possible to put many more systems simultaneously in the yeast genome, but we need to better understand and mitigate the impact of carrying heterologous regulators. There has been promising recent work to apply biophysics and control theory to this problem and it may be possible in the future to expand the complexity of the systems carried in yeast.[127,128]

In this manuscript, we applied our system to a problem of metabolic optimization for linalool production and show how it can be used to identify the optimal expression levels and timing. Optimization requires only making a single strain containing the pathway and then growing cells in different combinations of inducer concentration. A relatively simple optimization required 32 strains, corresponding to ∼1 MB of DNA construction if we altered expression levels by changing the physical DNA parts assigned to each gene, which we have done previously in yeast and bacteria.[34,36,38] Further, we used the system to quantify when different enzymes need to be induced, which could be used to guide the design of genetic circuits that turn on at the needed times without the addition of inducers. These data demonstrate the benefit of inducing all of the enzymes simultaneously with a slight delay to allow for growth to initiate before enzymes are expressed. We did not observe the need to stage more complex delays in gene expression that have been observed for other systems and "just-in-time" expression.[81,129,130] However, this could be due to us only evaluating gene expression delays in large and discrete timesteps of 2−4 h.

Automated strain construction is rapidly becoming the norm in the field.[39,44,131] With advances in acoustic liquid handlers that enable the mixing of picoliter droplets, it may be possible to automate the generation of each round of combinatorial inducer testing. This advance would make it possible to rapidly iterate through as many variants as could be analytically evaluated, perhaps using the guidance of search algorithms in selecting new rounds of combinatorics to be tested. This possibility speaks to a future where strains are developed specifically to work with high-throughput automation platforms to enable rapid searches through the complexity of multiparameter genetic search spaces.

METHODS

Strains, Media, and Chemicals. The strains were based on *S. cerevisiae* BY4741 *MATa his3Δ1 leu2Δ0 met15Δ0 ura3Δ0*. For transformation and outgrowth, yeast was grown in YPD broth (10 g/L yeast extract, BD Bacto #212750; 20 g/L peptone, BD Bacto #211677; 20 g/L glucose, Sigma-Aldrich #G8270-1KG). Linalool production was done in synthetic defined (SD) media (Sunrise #1701-500). Plasmid selections were done in either SD-Ura (Sunrise #1703-500) or SC/MSG with the antibiotic G418 (1.7 g/L Yeast Nitrogen Base without amino acids and ammonium sulfate, BD Difco #DF0335-15-9; 1 g/L Monosodium Glutamate; 2 g/L-Ura dropout mix, Sigma #Y1501-20; 20 g/L glucose, Sigma-Aldrich #G8270-1KG; 200 mg/L G418, Life Technologies Gibco #10131035). Cloning was done in chemically competent *E. coli* DH5α (NEB #C2987G), grown in LB Miller media (BD Difco #244610), supplemented with the appropriate antibiotic for selection (100 mg/L Carbenicillin, Gold Bio #C-103-5; 50 mg/L

https://doi.org/10.1021/acssynbio.2c00607
ACS Synth. Biol. 2023, 12, 1119−1132

Kanamycin, Gold Bio #K-120-5; 35 mg/L Chloramphenicol, VWR #AAB20841-14). Blue/white screening was done by adding 200 mg/L X-gal (VWR #100217-096) and 1 mM IPTG (Gold Bio #I2481C) to LB agar plates. The inducers used were IPTG (Gold Bio #I2481C), stocked as a 1 M solution in water; D-xylose (Xyl; Sigma-Aldrich #X1500), stocked as a 1 M solution in water; anhydrotetracycline hydrochloride (aTc; Sigma-Aldrich #37919), stocked as a 100 mg/L solution in dimethylformamide (Sigma-Aldrich #227056-1L); vanillic acid (Sigma-Aldrich #94770), stocked as a 100 mM solution in dimethylformamide; and galactose (Sigma-Aldrich #G0750), stocked as a 20% solution in water. The yellow fluorescent protein YFP (yEmCitrine) was used as the reporter.[132]

Plasmids and Cloning. Sensor and pathway constructs to be integrated into the genome were built using hierarchical assembly.[38] Individual parts (promoters, genes, terminators) were maintained as level 0 backbones. Promoters were maintained in the pEMY07AB backbone, flanked by *Bsa*I sites and the scars "A" (GTGC) and "B" (AATG). Genes were maintained in the pEMY07BC backbone, flanked by *Bsa*I sites and the scars "B" (AATG) and "C" (TAAA). Terminators were maintained in the pEMY07CD backbone, flanked by *Bsa*I sites and the scars "C" (TAAA) and "D" (CCTC). Promoters (Table S5), genes (Table S6), and terminators (Table S7) were then assembled using Type IIS assembly, *Bsa*I (NEB #R0535L), and high concentration T4 ligase (Promega #M1794) into the pDSMB backbones. Each pDSMB backbone contains upstream and downstream 50 bp connectors and map to a specific pathway position. The first position is linked to pDSMB1, the second to pDSMB2, the third to pDSMB3, and the fourth to pDSMB4. Each pDSMB transcription unit was then PCR-amplified, and the purified fragments were used for assembly using yeast homologous recombination. The upstream and downstream connectors work as overlaps for homologous recombination to assemble the transcription units together. The upstream connector of the first transcription unit and the downstream connector of the last transcription unit were amplified with 50 bp overhangs homologous to the target locus for genome integration. The pCfB2312 (TEF1p-Cas9-CYC1t) plasmid was a gift from Irina Borodina (Addgene plasmid #83946).[133] Genome-targeting gRNAs were cloned using Gibson assembly into the p426-SNR52p-gRNA.-CAN1.Y-SUP4t plasmid, a gift from George Church (Addgene plasmid #43803).[99]

Yeast Transformation and Genomic Integration. Yeast competent cells were prepared fresh for every transformation using a modified lithium acetate method.[134] A 25 mL yeast starter culture in YPD broth was incubated at 30 °C for 24 h, shaking at 250 rpm in a New Brunswick Innova 44 Shaker (Eppendorf). This starter culture was used to inoculate 100 mL of YPD media at a starting OD_{600} = 0.2. After 3 h of growth (OD_{600} between 0.4 and 0.6), cells were harvested by centrifugation at 1500*g* for 5 min and washed with sterile water. After a second centrifugation step, the pellet was resuspended in 0.5 mL of LiAc/TE solution (0.1 M lithium acetate, Sigma #L-6883; 10 mM Tris-HCl, Thermo Scientific #AM9856; and 1 mM EDTA, USB #15694). 0.1 mL of competent cells was added to a mixture containing the target DNA and 0.1 mg of denatured salmon sperm DNA (Thermo Fisher Scientific #15632011). Then, 0.6 mL of freshly prepared PEG/LiAc solution (40% w/v PEG 4000, Sigma, # 95904; 0.1 M lithium acetate, Sigma #L-6883; 10 mM Tris-HCl and 1 mM EDTA) was added to each transformation and vortexed for 10 s. Transformations were incubated at 30 °C for 1 h and then 70 μL of DMSO (Sigma #D8418-100) was added. The solution was then heat shocked at 42 °C in a water bath for 15 min followed by ice for 5 min. Then, 0.6 mL of TE was added to each tube (10 mM Tris-HCl and 1 mM EDTA) and cells were harvested by centrifuging at 13 000*g* for 15 s. The pellet was resuspended in 1 mL of YPD media, recovered at 30 °C for 1 h, and plated in the appropriate selective media. For genomic integrations, yeast was first transformed with the pCfB2312 plasmid[133] (TEF1p-Cas9-CYC1t) and selected on YPD and G418. Then, the pretransformed strain was grown in YPD media and G418 and 500 ng of each target fragment (amplified from the pDSMB backbones) were mixed with 200 ng of the gRNA plasmid targeting the desired genomic locus. Transformed strains were then selected on agar plates (SC/MSG-Ura and G418). Two genomic loci were targeted for integration (INT1 and INT2) (Figure S1).

Growth and Response Function Measurement. Each strain harboring the sensor array was streaked from glycerol stocks on YPD agar plates and grown overnight at 30 °C. A single colony was picked into 500 μL of SD media in a 2-mL-96-deep-well plate (Plate One #1896-2000) with a permeable seal (AeraSeal film, Excel Scientific #BS25). The plates were incubated at 30 °C in a Multitron Pro Incubator Shaker (INFORS HT) at 900 rpm for 24 h. From this, a 2.5 μL aliquot was used to inoculate 475.5 μL of fresh SD media (OD_{600} = 0.005) with the appropriate inducers in a 2-mL 96-deep-well deep well plates sealed with an AeraSeal film. The cultures were incubated at 30 °C in a Multitron Pro Incubator Shaker at 900 rpm for 24 h. After growth, the culture was diluted 10× in phosphate-buffered saline (PBS; Omnipur #6505-OP) containing 10 mg/L cycloheximide (Sigma-Aldrich #227048) in a 96-well U-bottom plate (Corning #3367) and incubated at room temperature for 1 h.

Flow Cytometry. Fluorescence was measured for >40 000 cells per sample using an LSRII Fortessa flow cytometer with HTS (BD Biosciences). Data were processed with custom Python scripts using the FlowCal[88] package and were gated by the forward scatter and the side scatter (FSC-W/SSC-W). The FITC-A channel was used to measure YFP fluorescence, calculated as the geometric mean of the distribution. When presented in arbitrary units, the background fluorescence of white cells (*S. cerevisiae* BY4741, YFP_0) is subtracted. To convert au to RPU, we measured RPU reference strain (*S. cerevisiae* CY671int, YFP_{RPU}), and this value was calculated by $RPU = (YFP - YFP_0)/(YFP_{RPU} - YFP_0)$.[56] The mean fluorescence values of the white cells and the RPU strain were 41 and 649 (AU), respectively.

Growth Measurements. For the growth curves reported in Figure 2f, growth was monitored by cell density (OD_{600}) using a Cary 60 UV−vis spectrophotometer (Agilent) with a cuvette of 1 cm path length. Cultures were diluted in the same media. The growth rates of strains harboring the sensor array and linalool pathways reported in Figure 3b and Note S1 were monitored in the same method with a Synergy H1 plate reader (BioTek). Culture aliquots were taken and diluted into the same media into a 96-well black-walled optical plate (Nunc #165305).

Linalool Pathway Construction. The IDI gene was amplified from the genome of *S. cerevisiae* BY4741. The tHMGR gene amplified from the HMG-CoA reductase (HMG1) gene from *S. cerevisiae* BY4741 truncated at amino acid 529. The ERG20 gene was codon-optimized for *S.*

https://doi.org/10.1021/acssynbio.2c00607
ACS Synth. Biol. 2023, 12, 1119−1132

cerevisiae and obtained using DNA synthesis (IDT) synthesized with the mutations N96W and N127W. LIS from *M. citrata* was codon-optimized for *S. cerevisiae*, truncated at amino acid 67 (t67-McLIS). The sequences are provided in Table S8.

Linalool Production and Quantification by GC-MS. Each strain harboring linalool pathways was directly inoculated from frozen glycerol stock and grown for 24 h in SD media at 30 °C shaking at 250 rpm in a New Brunswick Innova 44 Shaker. The culture was then used to inoculate 10 mL of SD media in 50 mL Falcon tubes (Corning #352070) to an initial OD_{600} = 0.05. For the experiments in Figure 2c, inducers were added after 8 h of growth. The cultures were grown at 30 °C shaking at 250 rpm in a New Brunswick Innova 44 Shaker for 48 h. Then, 500 μL of culture was transferred to a GC-vial (10 mL headspace vial, Supelco #SU860099), capped (Leap Pal #18031414), and immediately frozen at −80 °C. Prior to analysis, samples were thawed and the following were added: 1 μL of the Caryophyllene (Sigma-Aldrich # 22075) to a final concentration of 10 ppb, and 499 μL of 5 M $CaCl_2$ (Sigma #C7902). Caryophyllene serves as the internal standard. Samples were immediately capped and analyzed by GC-MS. Linalool was measured through SPME using an 85 μm CAR/PDMS fiber assembly (Supelco #57295) in an Agilent 7890A GC system with an Agilent 5975C MSD. The system is coupled with an Agilent PAL autosampler (GC Sampler 80). Each vial was preincubated at 50 °C for 10 min on the autosampler, and volatiles were extracted by exposing the SPME fiber to the vial headspace for 20 min at 50 °C. The fiber was desorbed for 2 min at the GC inlet (250 °C). Chromatography was done using He as a carrier gas at a constant flow rate of 1 mL/min in an HP-5ms GC column (30 m, 0.25 mm, 0.25 μm, Agilent #19091S-433). The oven temperature was held at 60 °C for 5 min, then ramped at 5 °C/min to 120 °C, then ramped at 25 °C/min to 250 °C and held at 250 °C for 2 min. The solvent delay was set to 5 min. Linalool was monitored using SIM mode on the *m/z* ions 80, 93, and 121. The internal standard Caryophyllene was monitored using SIM mode on the *m/z* ions 79 and 161. Peak areas were calculated using MSD ChemStation (Agilent). A leaner calibration curve was obtained using linalool standard (analytical grade, Sigma-Aldrich #74856—1 mL). Standard samples were prepared and measured by same method described above with different linalool concentrations (0, 1, 3, 5, 7, and 10 ng/mL). Each linalool concentration corresponded to peak area ratio calculated by dividing the linalool peak area by the Caryophyllene peak area in the calibration curve graph (Figure S6). A minimum of three experiments were performed on different days.

Modeling. The differential equations were solved as an initial value problem using the Newton−Cotes quadrature algorithm, encoded in python (https://github.com/VoigtLab/linalool_pathway_simulation). Enzymes and metabolites were defined as classes, initial values for metabolite concentrations were set at 0, and enzyme concentrations were set at $[E] = \alpha y_{\min}{}^{i}/\gamma$, where i refers to the corresponding inducible promoter P_i (see eq 3). Each run was started at OD_{600} = 0.005, and integrations were calculated numerically with timesteps of Δt = 0.001 min until reaching the corresponding end cell concentration (OD_{600} = 7.0).

■ ASSOCIATED CONTENT

Supporting Information

The Supporting Information is available free of charge at https://pubs.acs.org/doi/10.1021/acssynbio.2c00607.

Sensor specification sheets (Note S1); genomic loci used in this study (Figure S1); orthogonality of inducible systems (Figure S2); linalool production dynamics (Figure S3); strengths of promoters used to build the constitutive linalool pathway (Figure S4); sensor response when induced at different times (Figure S5); calibration curve to calculate linalool titers (Figure S6); plasmids and strains used in this study (Tables S1 and S2); experimental data of linalool production (Tables S3 and S4); and gene sequences used in this study (Tables S5−S8) (PDF)

■ AUTHOR INFORMATION

Corresponding Author

Christopher A. Voigt − *Synthetic Biology Center, Department of Biological Engineering, Massachusetts Institute of Technology, Cambridge, Massachusetts 02139, United States;* orcid.org/0000-0003-0844-4776; Email: cavoigt@gmail.com

Authors

Jong Hyun Park − *Synthetic Biology Center, Department of Biological Engineering, Massachusetts Institute of Technology, Cambridge, Massachusetts 02139, United States*

Marcelo C. Bassalo − *Synthetic Biology Center, Department of Biological Engineering, Massachusetts Institute of Technology, Cambridge, Massachusetts 02139, United States*

Geng-Min Lin − *Synthetic Biology Center, Department of Biological Engineering, Massachusetts Institute of Technology, Cambridge, Massachusetts 02139, United States;* orcid.org/0000-0001-8123-0921

Ye Chen − *Synthetic Biology Center, Department of Biological Engineering, Massachusetts Institute of Technology, Cambridge, Massachusetts 02139, United States*

Hamid Doosthosseini − *Synthetic Biology Center, Department of Biological Engineering, Massachusetts Institute of Technology, Cambridge, Massachusetts 02139, United States*

Joep Schmitz − *DSM Science & Innovation, Biodata & Translational Sciences, 2600 MA Delft, The Netherlands*

Johannes A. Roubos − *DSM Science & Innovation, Biodata & Translational Sciences, 2600 MA Delft, The Netherlands*

Complete contact information is available at: https://pubs.acs.org/10.1021/acssynbio.2c00607

Author Contributions

J.H.P. and M.C.B. carried out the experimental work and contributed to experimental design and data analysis. G.-M.L. performed the GC-MS and analyzed data. Y.C. involved in the conception and design. H.D. carried out simulations and modeling. J.S. and J.A.R. participated in the support and coordination of the project. J.H.P., M.C.B., and C.A.V. wrote the paper. C.A.V. contributed to experimental design and data analysis, and supervised this research. All authors read and approved the final version of the manuscript.

Notes

The authors declare no competing financial interest.

https://doi.org/10.1021/acssynbio.2c00607
ACS Synth. Biol. 2023, 12, 1119−1132

■ ACKNOWLEDGMENTS

This work was supported by funding from the US Defense Advanced Research Projects Agency (DARPA) Living Foundries program (Award HR0011-15-C-0084) and US Department of Energy Biological and Environmental Research (BER) program (Award DE-SC0018368).

■ REFERENCES

(1) Jensen, M. K.; Keasling, J. D. Recent applications of synthetic biology tools for yeast metabolic engineering. *FEMS Yeast Res.* **2015**, *15*, 1−10.
(2) Borodina, I.; Nielsen, J. Advances in metabolic engineering of yeast Saccharomyces cerevisiae for production of chemicals. *Biotechnol. J.* **2014**, *9*, 609−620.
(3) Ro, D. K.; Paradise, E. M.; Ouellet, M.; Fisher, K. J.; Newman, K. L.; Ndungu, J. M.; Ho, K. A.; Eachus, R. A.; Ham, T. S.; Kirby, J.; Chang, M. C. Y.; Withers, S. T.; Shiba, Y.; Sarpong, R.; Keasling, J. D. Production of the antimalarial drug precursor artemisinic acid in engineered yeast. *Nature* **2006**, *440*, 940−943.
(4) Westfall, P. J.; Pitera, D. J.; Lenihan, J. R.; Eng, D.; Woolard, F. X.; Regentin, R.; Horning, T.; Tsuruta, H.; Melis, D. J.; Owens, A.; Fickes, S.; Diola, D.; Benjamin, K. R.; Keasling, J. D.; Leavell, M. D.; McPhee, D. J.; Renninger, N. S.; Newman, J. D.; Paddon, C. J. Production of amorphadiene in yeast, and its conversion to dihydroartemisinic acid, precursor to the antimalarial agent artemisinin. *Proc. Natl. Acad. Sci. U.S.A.* **2012**, *109*, 111−118.
(5) Meadows, A. L.; Hawkins, K. M.; Tsegaye, Y.; Antipov, E.; Kim, Y.; Raetz, L.; Dahl, R. H.; Tai, A.; Mahatdejkul-Meadows, T.; Xu, L.; Zhao, L. S.; Dasika, M. S.; Murarka, A.; Lenihan, J.; Eng, D.; Leng, J. S.; Liu, C. L.; Wenger, J. W.; Jiang, H. X.; Chao, L. L.; Westfall, P.; Lai, J.; Ganesan, S.; Jackson, P.; Mans, R.; Platt, D.; Reeves, C. D.; Saija, P. R.; Wichmann, G.; Holmes, V. F.; Benjamin, K.; Hill, P. W.; Gardner, T. S.; Tsong, A. E. Rewriting yeast central carbon metabolism for industrial isoprenoid production. *Nature* **2016**, *537*, 694.
(6) Thodey, K.; Galanie, S.; Smolke, C. D. A microbial biomanufacturing platform for natural and semisynthetic opioids. *Nat. Chem. Biol.* **2014**, *10*, 837.
(7) Srinivasan, P.; Smolke, C. D. Biosynthesis of medicinal tropane alkaloids in yeast. *Nature* **2020**, *585*, 614.
(8) Payne, J. T.; Valentic, T. R.; Smolke, C. D. Complete biosynthesis of the bisbenzylisoquinoline alkaloids guattegaumerine and berbamunine in yeast. *Proc. Natl. Acad. Sci. U.S.A.* **2021**, *118*, No. e2112520118.
(9) Li, Y. R.; Smolke, C. D. Engineering biosynthesis of the anticancer alkaloid noscapine in yeast. *Nat. Commun.* **2016**, *7*, No. 12137.
(10) Paddon, C. J.; Keasling, J. D. Semi-synthetic artemisinin: a model for the use of synthetic biology in pharmaceutical development. *Nat. Rev. Microbiol.* **2014**, *12*, 355−367.
(11) Nielsen, J.; Keasling, J. D. Engineering Cellular Metabolism. *Cell* **2016**, *164*, 1185−1197.
(12) Naseri, G.; Koffas, M. A. G. Application of combinatorial optimization strategies in synthetic biology. *Nat. Commun.* **2020**, *11*, No. 2446.
(13) Du, J.; Shao, Z. Y.; Zhao, H. M. Engineering microbial factories for synthesis of value-added products. *J. Ind. Microbiol. Biotechnol.* **2011**, *38*, 873−890.
(14) Du, J.; Yuan, Y. B.; Si, T.; Lian, J. Z.; Zhao, H. M. Customized optimization of metabolic pathways by combinatorial transcriptional engineering. *Nucleic Acids Res.* **2012**, *40*, No. e142.
(15) Rugbjerg, P.; Sommer, M. O. A. Overcoming genetic heterogeneity in industrial fermentations. *Nat. Biotechnol.* **2019**, *37*, 869−876.
(16) Momen-Roknabadi, A.; Oikonomou, P.; Zegans, M.; Tavazoie, S. An inducible CRISPR interference library for genetic interrogation of Saccharomyces cerevisiae biology. *Commun. Biol.* **2020**, *3*, No. 723.
(17) Peng, K.; Kroukamp, H.; Pretorius, I. S.; Paulsen, I. T. Yeast Synthetic Minimal Biosensors for Evaluating Protein Production. *ACS Synth. Biol.* **2021**, *10*, 1640−1650.
(18) Peng, B. Y.; Bandari, N. C.; Lu, Z. Y.; Howard, C. B.; Scott, C.; Trau, M.; Dumsday, G.; Vickers, C. E. Engineering eukaryote-like regulatory circuits to expand artificial control mechanisms for metabolic engineering in Saccharomyces cerevisiae. *Commun. Biol.* **2022**, *5*, No. 135.
(19) Blazeck, J.; Garg, R.; Reed, B.; Alper, H. S. Controlling promoter strength and regulation in Saccharomyces cerevisiae using synthetic hybrid promoters. *Biotechnol. Bioeng.* **2012**, *109*, 2884−2895.
(20) Cuperus, J. T.; Groves, B.; Kuchina, A.; Rosenberg, A. B.; Jojic, N.; Fields, S.; Seelig, G. Deep learning of the regulatory grammar of yeast 5 ′ untranslated regions from 500,000 random sequences. *Genome Res.* **2017**, *27*, 2015−2024.
(21) Curran, K. A.; Crook, N. C.; Karim, A. S.; Gupta, A.; Wagman, A. M.; Alper, H. S. Design of synthetic yeast promoters via tuning of nucleosome architecture. *Nat. Commun.* **2014**, *5*, No. 4002.
(22) Guo, Y. K.; Dong, J. K.; Zhou, T.; Auxillos, J.; Li, T. Y.; Zhang, W. M.; Wang, L. H.; Shen, Y.; Luo, Y. S.; Zheng, Y. J.; Lin, J. W.; Chen, G. Q.; Wu, Q. Y.; Cai, Y. Z.; Dai, J. B. YeastFab: the design and construction of standard biological parts for metabolic engineering in Saccharomyces cerevisiae. *Nucleic Acids Res.* **2015**, *43*, No. e88.
(23) Kotopka, B. J.; Smolke, C. D. Model-driven generation of artificial yeast promoters. *Nat. Commun.* **2020**, *11*, No. 2113.
(24) Besada-Lombana, P. B.; McTaggart, T. L.; Da Silva, N. A. Molecular tools for pathway engineering in Saccharomyces cerevisiae. *Curr. Opin. Biotechnol.* **2018**, *53*, 39−49.
(25) Tang, H. T.; Wu, Y. L.; Deng, J. L.; Chen, N. Z.; Zheng, Z. H.; Wei, Y. J.; Luo, X. Z.; Keasling, J. D. Promoter Architecture and Promoter Engineering in Saccharomyces cerevisiae. *Metabolites* **2020**, *10*, No. 320.
(26) Curran, K. A.; Morse, N. J.; Markham, K. A.; Wagman, A. M.; Gupta, A.; Alper, H. S. Short Synthetic Terminators for Improved Heterologous Gene Expression in Yeast. *ACS Synth. Biol.* **2015**, *4*, 824−832.
(27) Decoene, T.; Peters, G.; De Maeseneire, S. L.; De Mey, M. Toward Predictable 5 ′ UTRs in Saccharomyces cerevisiae: Development of a yUTR Calculator. *ACS Synth. Biol.* **2018**, *7*, 622−634.
(28) Nevoigt, E.; Kohnke, J.; Fischer, C. R.; Alper, H.; Stahl, U.; Stephanopoulos, G. Engineering of promoter replacement cassettes for fine-tuning of gene expression in Saccharomyces cerevisiae. *Appl. Environ. Microbiol.* **2006**, *72*, 5266−5273.
(29) Casini, A.; Chang, F. Y.; Eluere, R.; King, A. M.; Young, E. M.; Dudley, Q. M.; Karim, A.; Pratt, K.; Bristol, C.; Forget, A.; Ghodasara, A.; Warden-Rothman, R.; Gan, R.; Cristofaro, A.; Borujeni, A. E.; Ryu, M. H.; Li, J.; Kwon, Y. C.; Wang, H.; Tatsis, E.; Rodriguez-Lopez, C.; O'Connor, S.; Medema, M. H.; Fischbach, M. A.; Jewett, M. C.; Voigt, C.; Gordon, D. B. A Pressure Test to Make 10 Molecules in 90 Days: External Evaluation of Methods to Engineer Biology. *J. Am. Chem. Soc.* **2018**, *140*, 4302−4316.
(30) Burén, S.; Young, E. M.; Sweeny, E. A.; Lopez-Torrejon, G.; Veldhuizen, M.; Voigt, C. A.; Rubio, L. M. Formation of Nitrogenase NifDK Tetramers in the Mitochondria of Saccharomyces cerevisiae. *ACS Synth. Biol.* **2017**, *6*, 1043−1055.
(31) Portela, R. M. C.; Vogl, T.; Kniely, C.; Fischer, J. E.; Oliveira, R.; Glieder, A. Synthetic Core Promoters as Universal Parts for Fine-Tuning Expression in Different Yeast Species. *ACS Synth. Biol.* **2017**, *6*, 471−484.
(32) Gao, S.; Zhou, H. R.; Zhou, J. W.; Chen, J. Promoter-Library-Based Pathway Optimization for Efficient (2S)-Naringenin Production from p-Coumaric Acid in Saccharomyces cerevisiae. *J. Agric. Food Chem.* **2020**, *68*, 6884−6891.
(33) Farasat, I.; Kushwaha, M.; Collens, J.; Easterbrook, M.; Guido, M.; Salis, H. M. Efficient search, mapping, and optimization of multi-protein genetic systems in diverse bacteria. *Mol. Syst. Biol.* **2014**, *10*, No. 731.

https://doi.org/10.1021/acssynbio.2c00607
ACS Synth. Biol. 2023, 12, 1119−1132

(34) Smanski, M. J.; Bhatia, S.; Zhao, D. H.; Park, Y.; Woodruff, L. B. A.; Giannoukos, G.; Ciulla, D.; Busby, M.; Calderon, J.; Nicol, R.; Gordon, D. B.; Densmore, D.; Voigt, C. A. Functional optimization of gene clusters by combinatorial design and assembly. *Nat. Biotechnol.* **2014**, *32*, 1241−1249.
(35) Ng, C. Y.; Farasat, I.; Maranas, C. D.; Salis, H. M. Rational design of a synthetic Entner-Doudoroff pathway for improved and controllable NADPH regeneration. *Metab. Eng.* **2015**, *29*, 86−96.
(36) Zhou, H.; Vonk, B.; Roubos, J. A.; Bovenberg, R. A. L.; Voigt, C. A. Algorithmic co-optimization of genetic constructs and growth conditions: application to 6-ACA, a potential nylon-6 precursor. *Nucleic Acids Res.* **2015**, *43*, 10560−10570.
(37) Jeschek, M.; Gerngross, D.; Panke, S. Combinatorial pathway optimization for streamlined metabolic engineering. *Curr. Opin. Biotechnol.* **2017**, *47*, 142−151.
(38) Young, E. M.; Zhao, Z.; Gielesen, B. E. M.; Wu, L.; Gordon, D. B.; Roubos, J. A.; Voigt, C. A. Iterative algorithm-guided design of massive strain libraries, applied to itaconic acid production in yeast. *Metab. Eng.* **2018**, *48*, 33−43.
(39) Carbonell, P.; Radivojevic, T.; Martin, H. G. Opportunities at the Intersection of Synthetic Biology, Machine Learning, and Automation. *ACS Synth. Biol.* **2019**, *8*, 1474−1477.
(40) Zhang, C.; Seow, V. Y.; Chen, X.; Too, H. P. Multidimensional heuristic process for high-yield production of astaxanthin and fragrance molecules in Escherichia coli. *Nat. Commun.* **2018**, *9*, No. 1858.
(41) Chambers, S.; Kitney, R.; Freemont, P. The Foundry: the DNA synthesis and construction Foundry at Imperial College. *Biochem. Soc. Trans.* **2016**, *44*, 687−688.
(42) Kanigowska, P.; Shen, Y.; Zheng, Y. J.; Rosser, S.; Cai, Y. Z. Smart DNA Fabrication Using Sound Waves: Applying Acoustic Dispensing Technologies to Synthetic Biology. *SLAS Technol.* **2016**, *21*, 49−56.
(43) Chao, R.; Liang, J.; Tasan, I.; Si, T.; Ju, L. Y.; Zhao, H. M. Fully Automated One-Step Synthesis of Single-Transcript TALEN Pairs Using a Biological Foundry. *ACS Synth. Biol.* **2017**, *6*, 678−685.
(44) Zhang, J. Z.; Chen, Y. C.; Fu, L. H.; Guo, E. P.; Wang, B.; Dai, L.; Si, T. Accelerating strain engineering in biofuel research via build and test automation of synthetic biology. *Curr. Opin. Biotechnol.* **2021**, *67*, 88−98.
(45) Chou, H. H.; Keasling, J. D. Programming adaptive control to evolve increased metabolite production. *Nat. Commun.* **2013**, *4*, No. 2595.
(46) Ottoz, D. S. M.; Rudolf, F.; Stelling, J. Inducible, tightly regulated and growth condition-independent transcription factor in Saccharomyces cerevisiae. *Nucleic Acids Res.* **2014**, *42*, No. e130.
(47) Mukherjee, K.; Bhattacharyya, S.; Peralta-Yahya, P. GPCR-Based Chemical Biosensors for Medium-Chain Fatty Acids. *ACS Synth. Biol.* **2015**, *4*, 1261−1269.
(48) Billerbeck, S.; Brisbois, J.; Agmon, N.; Jimenez, M.; Temple, J.; Shen, M.; Boeke, J. D.; Cornish, V. W. A scalable peptide-GPCR language for engineering multicellular communication. *Nat. Commun.* **2018**, *9*, No. 5057.
(49) Wang, X. S.; van Westen, G. J. P.; Heitman, L. H.; Ijzerman, A. P. G protein-coupled receptors expressed and studied in yeast. The adenosine receptor as a prime example. *Biochem. Pharmacol.* **2021**, *187*, No. 114370.
(50) Eldridge, M. L.; Sanseverino, J.; Layton, A. C.; Easter, J. P.; Schultz, T. W.; Sayler, G. S. Saccharomyces cerevisiae BLYAS, a new Bioluminescent bioreporter for detection of androgenic compounds. *Appl. Environ. Microbiol.* **2007**, *73*, 6012−6018.
(51) Kawanishi, M.; Ohnisi, K.; Takigami, H.; Yagi, T. Simple and rapid yeast reporter bioassay for dioxin screening: evaluation of the dioxin-like compounds in industrial and municipal waste incineration plants. *Environ. Sci. Pollut. Res.* **2013**, *20*, 2993−3002.
(52) Skjoedt, M. L.; Snoek, T.; Kildegaard, K. R.; Arsovska, D.; Eichenberger, M.; Goedecke, T. J.; Rajkumar, A. S.; Zhang, J.; Kristensen, M.; Lehka, B. J.; Siedler, S.; Borodina, I.; Jensen, M. K.; Keasling, J. D. Engineering prokaryotic transcriptional activators as metabolite biosensors in yeast. *Nat. Chem. Biol.* **2016**, *12*, 951.
(53) Qiu, C. X.; Zhai, H. T.; Hou, J. Biosensors design in yeast and applications in metabolic engineering. *FEMS Yeast Res.* **2019**, *19*, No. foz082.
(54) Marsafari, M.; Ma, J. B.; Koffas, M.; Xu, P. Genetically-encoded biosensors for analyzing and controlling cellular process in yeast. *Curr. Opin. Biotechnol.* **2020**, *64*, 175−182.
(55) Zhou, Y. K.; Yuan, Y. M.; Wu, Y. A.; Li, L.; Jameel, A.; Xing, X. H.; Zhang, C. Encoding Genetic Circuits with DNA Barcodes Paves the Way for Machine Learning-Assisted Metabolite Biosensor Response Curve Profiling in Yeast. *ACS Synth. Biol.* **2022**, *11*, 977−989.
(56) Chen, Y.; Zhang, S. Y.; Young, E. M.; Jones, T. S.; Densmore, D.; Voigt, C. A. Genetic circuit design automation for yeast. *Nat. Microbiol.* **2020**, *5*, 1349−1360.
(57) Feng, J.; Jester, B. W.; Tinberg, C. E.; Mandell, D. J.; Antunes, M. S.; Chari, R.; Morey, K. J.; Rios, X.; Medford, J. I.; Church, G. M.; Fields, S.; Baker, D. A general strategy to construct small molecule biosensors in eukaryotes. *eLife* **2015**, *4*, No. e10606.
(58) Belli, G.; Gari, E.; Piedrafita, L.; Aldea, N.; Herrero, E. An activator/repressor dual system allows tight tetracycline-regulated gene expression in budding yeast. *Nucleic Acids Res.* **1998**, *26*, 942−947.
(59) Wei, W. P.; Shang, Y. Z.; Zhang, P.; Liu, Y.; You, D.; Yin, B. C.; Ye, B. C. Engineering Prokaryotic Transcriptional Activator XylR as a Xylose-Inducible Biosensor for Transcription Activation in Yeast. *ACS Synth. Biol.* **2020**, *9*, 1022−1029.
(60) Snoek, T.; Chaberski, E. K.; Ambri, F.; Kol, S.; Bjorn, S. P.; Pang, B.; Barajas, J. F.; Welner, D. H.; Jensen, M. K.; Keasling, J. D. Evolution-guided engineering of small-molecule biosensors. *Nucleic Acids Res.* **2020**, *48*, No. e3.
(61) Ikushima, S.; Boeke, J. D. New Orthogonal Transcriptional Switches Derived from Tet Repressor Homologues for Saccharomyces cerevisiae Regulated by 2,4-Diacetylphloroglucinol and Other Ligands. *ACS Synth. Biol.* **2017**, *6*, 497−506.
(62) Ambri, F.; D'Ambrosio, V.; Di Blasi, R.; Maury, J.; Jacobsen, S. A. B.; McCloskey, D.; Jensen, M. K.; Keasling, J. D. High-Resolution Scanning of Optimal Biosensor Reporter Promoters in Yeast. *ACS Synth. Biol.* **2020**, *9*, 218−226.
(63) Tominaga, M.; Nozaki, K.; Umeno, D.; Ishii, J.; Kondo, A. Robust and flexible platform for directed evolution of yeast genetic switches. *Nat. Commun.* **2021**, *12*, No. 1846.
(64) Nasr, M. A.; Timmins, L. R.; Martin, V. J. J.; Kwan, D. H. A Versatile Transcription Factor Biosensor System Responsive to Multiple Aromatic and Indole Inducers. *ACS Synth. Biol.* **2022**, *11*, 1692−1698.
(65) Sanford, A.; Kiriakov, S.; Khalil, A. S. A Toolkit for Precise, Multigene Control in Saccharomyces cerevisiae. *ACS Synth. Biol.* **2022**, *11*, 3912−3920.
(66) Nielsen, A. A. K.; Segall-Shapiro, T. H.; Voigt, C. A. Advances in genetic circuit design: novel biochemistries, deep part mining, and precision gene expression. *Curr. Opin. Chem. Biol.* **2013**, *17*, 878−892.
(67) Stanton, B. C.; Nielsen, A. A. K.; Tamsir, A.; Clancy, K.; Peterson, T.; Voigt, C. A. Genomic mining of prokaryotic repressors for orthogonal logic gates. *Nat. Chem. Biol.* **2014**, *10*, 99−105.
(68) Rantasalo, A.; Kuivanen, J.; Penttila, M.; Jantti, J.; Mojzita, D. Synthetic Toolkit for Complex Genetic Circuit Engineering in Saccharomyces cerevisiae. *ACS Synth. Biol.* **2018**, *7*, 1573−1587.
(69) Stanton, B. C.; Siciliano, V.; Ghodasara, A.; Wroblewska, L.; Clancy, K.; Trefzer, A. C.; Chesnut, J. D.; Weiss, R.; Voigt, C. A. Systematic Transfer of Prokaryotic Sensors and Circuits to Mammalian Cells. *ACS Synth. Biol.* **2014**, *3*, 880−891.
(70) Bashor, C. J.; Patel, N.; Choubey, S.; Beyzavi, A.; Kondev, J.; Collins, J. J.; Khalil, A. S. Complex signal processing in synthetic gene circuits using cooperative regulatory assemblies. *Science* **2019**, *364*, 593.
(71) Kelly, J. R.; Rubin, A. J.; Davis, J. H.; Ajo-Franklin, C. M.; Cumbers, J.; Czar, M. J.; de Mora, K.; Glieberman, A. L.; Monie, D.

D.; Endy, D. Measuring the activity of BioBrick promoters using an in vivo reference standard. *J. Biol. Eng.* **2009**, *3*, 4.
(72) Canton, B.; Labno, A.; Endy, D. Refinement and standardization of synthetic biological parts and devices. *Nat. Biotechnol.* **2008**, *26*, 787−793.
(73) Shao, B.; Rammohan, J.; Anderson, D. A.; Alperovich, N.; Ross, D.; Voigt, C. A. Single-cell measurement of plasmid copy number and promoter activity. *Nat. Commun.* **2021**, *12*, No. 1475.
(74) Ghodasara, A.; Voigt, C. A. Balancing gene expression without library construction via a reusable sRNA pool. *Nucleic Acids Res.* **2017**, *45*, 8116−8127.
(75) Tan, S. Z.; Prather, K. L. J. Dynamic pathway regulation: recent advances and methods of construction. *Curr. Opin. Chem. Biol.* **2017**, *41*, 28−35.
(76) Ni, C.; Dinh, C. V.; Prather, K. L. J. Dynamic Control of Metabolism. *Annu. Rev. Chem. Biomol. Eng.* **2021**, *12*, 519−541.
(77) Xu, P. Production of chemicals using dynamic control of metabolic fluxes. *Curr. Opin. Biotechnol.* **2018**, *53*, 12−19.
(78) Varma, A.; Palsson, B. O. Metabolic Flux Balancing: Basic Concepts, Scientific and Practical Use. *Nat. Biotechnol.* **1994**, *12*, 994−998.
(79) Gupta, A.; Reizman, I. M. B.; Reisch, C. R.; Prather, K. L. J. Dynamic regulation of metabolic flux in engineered bacteria using a pathway-independent quorum-sensing circuit. *Nat. Biotechnol.* **2017**, *35*, 273.
(80) Moser, F.; Borujeni, A. E.; Ghodasara, A. N.; Cameron, E.; Park, Y.; Voigt, C. A. Dynamic control of endogenous metabolism with combinatorial logic circuits. *Mol. Syst. Biol.* **2018**, *14*, No. e8605.
(81) Zaslaver, A.; Mayo, A. E.; Rosenberg, R.; Bashkin, P.; Sberro, H.; Tsalyuk, M.; Surette, M. G.; Alon, U. Just-in-time transcription program in metabolic pathways. *Nat. Genet.* **2004**, *36*, 486−491.
(82) Kuang, Z.; Cai, L.; Zhang, X. K.; Ji, H. K.; Tu, B. P.; Boeke, J. D. High-temporal-resolution view of transcription and chromatin states across distinct metabolic states in budding yeast. *Nat. Struct. Mol. Biol.* **2014**, *21*, 854−863.
(83) Chubukov, V.; Zuleta, I. A.; Li, H. Regulatory architecture determines optimal regulation of gene expression in metabolic pathways. *Proc. Natl. Acad. Sci. U.S.A.* **2012**, *109*, 5127−5132.
(84) Amiri, P.; Shahpiri, A.; Asadollahi, M. A.; Momenbeik, F.; Partow, S. Metabolic engineering of Saccharomyces cerevisiae for linalool production. *Biotechnol. Lett.* **2016**, *38*, 503−508.
(85) Deng, Y.; Sun, M. X.; Xu, S.; Zhou, J. W. Enhanced (S)-linalool production by fusion expression of farnesyl diphosphate synthase and linalool synthase in Saccharomyces cerevisiae. *J. Appl. Microbiol.* **2016**, *121*, 187−195.
(86) Zhang, Y. Y.; Wang, J.; Cao, X. S.; Liu, W.; Yu, H. W.; Ye, L. D. High-level production of linalool by engineered Saccharomyces cerevisiae harboring dual mevalonate pathways in mitochondria and cytoplasm. *Enzyme Microb. Technol.* **2020**, *134*, No. 109462.
(87) Meylemans, H. A.; Quintana, R. L.; Goldsmith, B. R.; Harvey, B. G. Solvent-Free Conversion of Linalool to Methylcyclopentadiene Dimers: A Route To Renewable High-Density Fuels. *ChemSusChem* **2011**, *4*, 465−469.
(88) Mendez-Perez, D.; Alonso-Gutierrez, J.; Hu, Q. J.; Molinas, M.; Baidoo, E. E. K.; Wang, G.; Chan, L. J. G.; Adams, P. D.; Petzold, C. J.; Keasling, J. D.; Lee, T. S. Production of jet fuel precursor monoterpenoids from engineered Escherichia coli. *Biotechnol. Bioeng.* **2017**, *114*, 1703−1712.
(89) Baral, N. R.; Kavvada, O.; Mendez-Perez, D.; Mukhopadhyay, A.; Lee, T. S.; Simmons, B. A.; Scown, C. D. Techno-economic analysis and life-cycle greenhouse gas mitigation cost of five routes to bio-jet fuel blendstocks. *Energy Environ. Sci.* **2019**, *12*, 807−824.
(90) Woodroffe, J. D.; Harvey, B. G. High-Performance, Biobased, Jet Fuel Blends Containing Hydrogenated Monoterpenes and Synthetic Paraffinic Kerosenes. *Energy Fuels* **2020**, *34*, 5929−5937.
(91) Cao, X.; Wei, L. J.; Lin, J. Y.; Hua, Q. Enhancing linalool production by engineering oleaginous yeast Yarrowia lipolytica. *Bioresour. Technol.* **2017**, *245*, 1641−1644.
(92) Zhou, P. P.; Du, Y.; Fang, X.; Xu, N. N.; Yue, C. L.; Ye, L. D. Combinatorial Modulation of Linalool Synthase and Farnesyl Diphosphate Synthase for Linalool Overproduction in Saccharomyces cerevisiae. *J. Agric. Food Chem.* **2021**, *69*, 1003−1010.
(93) Vranová, E.; Coman, D.; Gruissem, W. Network Analysis of the MVA and MEP Pathways for Isoprenoid Synthesis. *Annu. Rev. Plant Biol.* **2013**, *64*, 665−700.
(94) Crowell, A. L.; Williams, D. C.; Davis, E. M.; Wildung, M. R.; Croteau, R. Molecular cloning and characterization of a new linalool synthase. *Arch. Biochem. Biophys.* **2002**, *405*, 112−121.
(95) Denby, C. M.; Li, R. A.; Vu, V.; Costello, Z.; Lin, W. Y.; Chan, L. J. G.; Williams, J.; Donaldson, B.; Bamforth, C. W.; Petzold, C. J.; Scheller, H. V.; Martin, H. G.; Keasling, J. D. Industrial brewing yeast engineered for the production of primary flavor determinants in hopped beer. *Nat. Commun.* **2018**, *9*, No. 965.
(96) Zhao, J. Z.; Bao, X. M.; Li, C.; Shen, Y.; Hou, J. Improving monoterpene geraniol production through geranyl diphosphate synthesis regulation in Saccharomyces cerevisiae. *Appl. Microbiol. Biotechnol.* **2016**, *100*, 4561−4571.
(97) Lv, X. M.; Wang, F.; Zhou, P. P.; Ye, L. D.; Xie, W. P.; Xu, H. M.; Yu, H. W. Dual regulation of cytoplasmic and mitochondrial acetyl-CoA utilization for improved isoprene production in Saccharomyces cerevisiae. *Nat. Commun.* **2016**, *7*, No. 12851.
(98) Cong, L.; Ran, F. A.; Cox, D.; Lin, S. L.; Barretto, R.; Habib, N.; Hsu, P. D.; Wu, X. B.; Jiang, W. Y.; Marraffini, L. A.; Zhang, F. Multiplex Genome Engineering Using CRISPR/Cas Systems. *Science* **2013**, *339*, 819−823.
(99) DiCarlo, J. E.; Norville, J. E.; Mali, P.; Rios, X.; Aach, J.; Church, G. M. Genome engineering in Saccharomyces cerevisiae using CRISPR-Cas systems. *Nucleic Acids Res.* **2013**, *41*, 4336−4343.
(100) Lou, C.; Stanton, B.; Chen, Y. J.; Munsky, B.; Voigt, C. A. Ribozyme-based insulator parts buffer synthetic circuits from genetic context. *Nat. Biotechnol.* **2012**, *30*, 1137−1142.
(101) Zong, Y.; Zhang, H. M.; Lyu, C.; Ji, X.; Hou, J.; Guo, X.; Ouyang, Q.; Lou, C. Insulated transcriptional elements enable precise design of genetic circuits. *Nat. Commun.* **2017**, *8*, No. 52.
(102) Baharum, S. N.; Bunawan, H.; Ghani, M. A.; Mustapha, W. A.; Noor, N. M. Analysis of the chemical composition of the essential oil of Polygonum minus Huds. using two-dimensional gas chromatography-time-of-flight mass spectrometry (GC-TOF MS). *Molecules* **2010**, *15*, 7006−7015.
(103) Rodriguez, S.; Kirby, J.; Denby, C. M.; Keasling, J. D. Production and quantification of sesquiterpenes in Saccharomyces cerevisiae, including extraction, detection and quantification of terpene products and key related metabolites. *Nat. Protoc.* **2014**, *9*, 1980−1996.
(104) Donald, K. A.; Hampton, R. Y.; Fritz, I. B. Effects of overproduction of the catalytic domain of 3-hydroxy-3-methylglutaryl coenzyme A reductase on squalene synthesis in Saccharomyces cerevisiae. *Appl. Environ. Microbiol.* **1997**, *63*, 3341−3344.
(105) Yao, Z.; Zhou, P.; Su, B.; Su, S.; Ye, L.; Yu, H. Enhanced Isoprene Production by Reconstruction of Metabolic Balance between Strengthened Precursor Supply and Improved Isoprene Synthase in Saccharomyces cerevisiae. *ACS Synth. Biol.* **2018**, *7*, 2308−2316.
(106) Liu, G. S.; Li, T.; Zhou, W.; Jiang, M.; Tao, X. Y.; Liu, M.; Zhao, M.; Ren, Y. H.; Gao, B.; Wang, F. Q.; Wei, D. Z. The yeast peroxisome: A dynamic storage depot and subcellular factory for squalene overproduction. *Metab. Eng.* **2020**, *57*, 151−161.
(107) Pitera, D. J.; Paddon, C. J.; Newman, J. D.; Keasling, J. D. Balancing a heterologous mevalonate pathway for improved isoprenoid production in Escherichia coli. *Metab. Eng.* **2007**, *9*, 193−207.
(108) Anthony, J. R.; Anthony, L. C.; Nowroozi, F.; Kwon, G.; Newman, J. D.; Keasling, J. D. Optimization of the mevalonate-based isoprenoid biosynthetic pathway in Escherichia coli for production of the anti-malarial drug precursor amorpha-4,11-diene. *Metab. Eng.* **2009**, *11*, 13−19.

https://doi.org/10.1021/acssynbio.2c00607
ACS Synth. Biol. 2023, 12, 1119−1132

(109) Martin, V. J. J.; Pitera, D. J.; Withers, S. T.; Newman, J. D.; Keasling, J. D. Engineering a mevalonate pathway in Escherichia coli for production of terpenoids. *Nat. Biotechnol.* **2003**, *21*, 796−802.
(110) George, K. W.; Thompso, M. G.; Kim, J.; Baidoo, E. E. K.; Wang, G.; Benites, V. T.; Petzold, C. J.; Chan, L. J. G.; Yilmaz, S.; Turhanen, P.; Adam, P. D.; Keasling, J. D.; Lee, T. S. Integrated analysis of isopentenyl pyrophosphate (IPP) toxicity in isoprenoid-producing Escherichia coli. *Metab. Eng.* **2018**, *47*, 60−72.
(111) Ghaemmaghami, S.; Huh, W.-K.; Bower, K.; Howson, R. W.; Belle, A.; Dephoure, N.; O'Shea, E. K.; Weissman, J. S. Global analysis of protein expression in yeast. *Nature* **2003**, *425*, 737−741.
(112) Milo, R.; Jorgensen, P.; Moran, U.; Weber, G.; Springer, M. BioNumbers—the database of key numbers in molecular and cell biology. *Nucleic Acids Res.* **2010**, *38*, D750−D753.
(113) Middleton, B. The kinetic mechanism of 3-hydroxy-3-methylglutaryl-coenzyme A synthase from baker's yeast. *Biochem. J.* **1972**, *126*, 35−47.
(114) Ma, S. M.; Garcia, D. E.; Redding-Johanson, A. M.; Friedland, G. D.; Chan, R.; Batth, T. S.; Haliburton, J. R.; Chivian, D.; Keasling, J. D.; Petzold, C. J.; et al. Optimization of a heterologous mevalonate pathway through the use of variant HMG-CoA reductases. *Metab. Eng.* **2011**, *13*, 588−597.
(115) Schomburg, I.; Chang, A.; Schomburg, D. BRENDA, enzyme data and metabolic information. *Nucleic Acids Res.* **2002**, *30*, 47−49.
(116) Durr, I.; Rudney, H. The reduction of *β*-hydroxy-*β*-methylglutaryl coenzyme A to mevalonic acid. *J. Biol. Chem.* **1960**, *235*, 2572−2578.
(117) Rubat, S.; Varas, I.; Sepúlveda, R.; Almonacid, D.; González-Nilo, F.; Agosin, E. Increasing the intracellular isoprenoid pool in Saccharomyces cerevisiae by structural fine-tuning of a bifunctional farnesyl diphosphate synthase. *FEMS Yeast Res.* **2017**, *17*, No. fox032.
(118) Ignea, C.; Pontini, M.; Maffei, M. E.; Makris, A. M.; Kampranis, S. C. Engineering monoterpene production in yeast using a synthetic dominant negative geranyl diphosphate synthase. *ACS Synth. Biol.* **2014**, *3*, 298−306.
(119) Cleland, W. W. Enzyme kinetics. *Annu. Rev. Biochem.* **1967**, *36*, 77−112.
(120) Alberty, R. A. The relationship between Michaelis constants, maximum velocities and the equilibrium constant for an enzyme-catalyzed reaction. *J. Am. Chem. Soc.* **1953**, *75*, 1928−1932.
(121) Street, I. P.; Coffman, H. R.; Poulter, C. D.; Baker, J. A. Identification of Cys139 and Glu207 as catalytically important groups in the active site of isopentenyl diphosphate: dimethylallyl diphosphate isomerase. *Biochemistry* **1994**, *33*, 4212−4217.
(122) Neti, S. S.; Pan, J.-J.; Poulter, C. D. Mechanistic Studies of the Protonation−Deprotonation Reactions for Type 1 and Type 2 Isopentenyl Diphosphate: Dimethylallyl Diphosphate Isomerase. *J. Am. Chem. Soc.* **2018**, *140*, 12900−12908.
(123) Lutz, R.; Bujard, H. Independent and tight regulation of transcriptional units in Escherichia coli via the LacR/O, the TetR/O and AraC/I1-I2 regulatory elements. *Nucleic Acids Res.* **1997**, *25*, 1203−1210.
(124) McAdams, H. H.; Arkin, A. Towards a circuit engineering discipline. *Curr. Biol.* **2000**, *10*, R318−R320.
(125) Gardner, T. S.; Cantor, C. R.; Collins, J. J. Construction of a genetic toggle switch in Escherichia coli. *Nature* **2000**, *403*, 339−342.
(126) Meyer, A. J.; Segall-Shapiro, T. H.; Glassey, E.; Zhang, J.; Voigt, C. A. Escherichia coli "Marionette" strains with 12 highly optimized small-molecule sensors. *Nat. Chem. Biol.* **2019**, *15*, 196.
(127) Del Vecchio, D.; Dy, A. J.; Qian, Y. Control theory meets synthetic biology. *J. R. Soc. Interface* **2016**, *13*, No. 20160380.
(128) McBride, C. D.; Grunberg, T. W.; Del Vecchio, D. Design of genetic circuits that are robust to resource competition. *Curr. Opin. Syst. Biol.* **2021**, *28*, No. 100357.
(129) Kalir, S.; McClure, J.; Pabbaraju, K.; Southward, C.; Ronen, M.; Leibler, S.; Surette, M. G.; Alon, U. Ordering genes in a flagella pathway by analysis of expression kinetics from living bacteria. *Science* **2001**, *292*, 2080−2083.
(130) Wagner, S.; Konigsmaier, L.; Lara-Tejero, M.; Lefebre, M.; Marlovits, T. C.; Galan, J. E. Organization and coordinated assembly of the type III secretion export apparatus. *Proc. Natl. Acad. Sci. U.S.A.* **2010**, *107*, 17745−17750.
(131) Clarke, L. J.; Kitney, R. I. Synthetic biology in the UK - An outline of plans and progress. *Synth. Syst. Biotechnol.* **2016**, *1*, 243−257.
(132) Sheff, M. A.; Thorn, K. S. Optimized cassettes for fluorescent protein tagging in Saccharomyces cerevisiae. *Yeast* **2004**, *21*, 661−670.
(133) Stovicek, V.; Borodina, I.; Forster, J. CRISPR-Cas system enables fast and simple genome editing of industrial Saccharomyces cerevisiae strains. *Metab. Eng. Commun.* **2015**, *2*, 13−22.
(134) Gietz, R. D.; Schiestl, R. H. Large-scale high-efficiency yeast transformation using the LiAc/SS carrier DNA/PEG method. *Nat. Protoc.* **2007**, *2*, 38−41.

https://doi.org/10.1021/acssynbio.2c00607
ACS Synth. Biol. 2023, 12, 1119−1132